Original Paper

Determination of Solubility Limits and Distribution Coefficients of Rare Earth Ln^{3+} Ions (Ln = Y, Ho, Eu or Nd) in $Ca_{12}Al_{14}O_{33}$ Crystals Using Floating Zone Growth

M. Mozahar ALI, Masanori NAGAO, Satoshi WATAUCHI, Isao TANAKA*

Center for Crystal Science and Technology, University of Yamanashi, 7-32 Miyamae, Kofu, Yamanashi 400-8511

Received July 13, 2016; E-mail: itanaka@yamanashi.ac.jp

We report the solubility limits and distribution coefficients of rare earth Ln^{3+} ions (Ln = Y, Ho, Eu or Nd) in $Ca_{12}Al_{14}O_{33}$ (C12A7) using the floating zone (FZ) crystal growth technique. The solubility limit of Ln^{3+} is estimated in the final region of the C12A7:Ln crystal cooled slowly after growth by this FZ method, with nominal concentrations of 1 or 2 at% Ln in the C12A7 feed. The solubility limits of Y, Ho, Eu and Nd in C12A7 were estimated to be 0.30(1), 0.48(2), 0.78(1) and 0.91(1) at%, respectively. These values agree with those determined using the lattice parameters of samples prepared using a more conventional solid state reaction method. The effective distribution coefficient of Ln in C12A7 was determined from the distribution of the Ln concentration along the growth direction at the initial growth region of C12A7:Ln crystals (grown at a growth rate of 1 mm·h^{-1} by FZ method). The effective distribution coefficients of Y, Ho, Eu and Nd were determined to be 0.105(12), 0.108(11), 0.075(7) and 0.142(15), respectively.

Key Words: *Floating Zone Technique, Solubility, C12A7 Crystal, Rare Earth Ion, Distribution Coefficient*

1. Introduction

Mayenite ($Ca_{12}Al_{14}O_{33}$, C12A7) is an electrical insulator composed of lime and alumina, and is used commercially as a component of aluminate cements in refractories, chemical resistant concretes, building products, sewers and so on [1-2]. The C12A7 crystal has a cage-like structure with a positive lattice framework containing 12 cages in a unit cell, with two extra framework O^{2-} ions occupying two of these cages. These extra framework O^{2-} ions (called free oxide ions) can be replaced by monovalent anions such as OH^-, H^-, Cl^-, F^-, Au^- as well as electrons (e^-) [3-7]. Anion-doped C12A7 crystals show unique features of light induced insulation, conductor conversion (for C12A7:H^-), insulator to metal transitions, and even a superconducting transition at 0.2 K for metallic C12A7:e^- [4,7-10]. As a result, this material has attracted keen interest for applications such as oxygen gas sensing, oxidation catalysis, and solid oxide fuel cells due to its unique structure [11,12]. Recently, electron doped C12A7:e^- electride has seen use in electronic devices as an electron emitting source or low electron injection barrier due to its low work function properties [13,14]. In high density electron-doped C12A7, electrons migrate through neighboring cages, creating high electrical conductivity. In order to understand the high electrical conductivity in C12A7:e^- however, a new design concept to dope high density electrons is required, which compensates for the positive charge of the insulating C12A7 lattice framework. Substitution of trivalent cations into divalent Ca^{2+} sites in C12A7 is one possible method for increasing the positive charge within the lattice framework. Rare earth (Ln) ion-doped C12A7:Ln phosphors, C12A7:Ho^{3+}, Tm^{3+}/Yb^{3+} polycrystals and C12A7:Eu thin films have been synthesized by solid state reaction methods and their optical properties widely investigated [15-19]. However, C12A7:Ln single crystals are needed in order to precisely measure several other important properties. To grow C12A7:Ln single crystals using melt growth, the solubility limit and distribution coefficient of Ln^{3+} for Ca^{2+} sites in C12A7 must be clarified.

2. Concept for determination of solubility limit and distribution coefficient

The floating zone (FZ) crystal growth technique was applied to determine solubility limits and distribution coefficients of solid solutions by compositional analyses of the slow cooling region and growth region of the FZ grown crystals. Figures 1 show schematic illustrations of phase diagram in solid solutions with the distribution coefficient $k < 1$ and the distribution of dopant concentration along the growth direction in the crystal grown by the FZ method.

The dopant concentration at the initial growth position is minimum and gradually increases as proceeds along the growth direction as shown in Fig.1(b). The profile of dopant concentration according to zone melting process is defined as the following equation [20,21]:

$$\frac{C(x)}{C_0} = 1 - (1 - k)\exp\left(-\frac{kx}{l}\right) \quad (1)$$

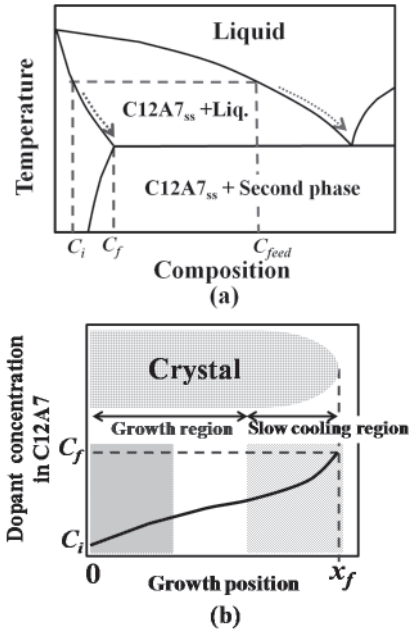

Fig.1 Schematic phase diagram (a), and dopant concentration along the growth direction in Ln-doped C12A7 crystal (b).

where k is the distribution coefficient, $C(x)$ is the crystal dopant concentration at distance x, C_0 is the dopant concentration of the feed rod, and l is the length of the molten zone. Therefore, the distribution coefficient is determined by measuring the distribution of dopant concentration $C(x)$ from the initial crystallization point along the growth direction in C12A7:Ln crystal grown using a Ln-doped feed of concentration C_0 (less than the eutectic composition) using electron probe micro-analyzer (EPMA).

During separation of the feed from the molten zone, we utilized a slow cooling floating zone (SCFZ) technique in which the temperature of the melt was slowly cooled, while the feed was simultaneously slowly detached from the melt. Finally, the remaining melt solidified completely at the top edge of the crystal upon further cooling; this entire process is analogous to a normal freezing process. In a normal freezing process, slow-cooling the molten zone after FZ crystal growth causes a gradual change of the dopant concentration towards the solubility limit C_f in the final part of the grown crystal, as shown in Fig.1(b). Therefore, the solubility limit is determined by measuring the maximum dopant concentration in the C12A7 phase at the final growth region using EPMA.

3. Experimental Procedure

$12Ca_{1-x}Ln_xO{\cdot}7Al_2O_3$ (Ln^{3+} = Y^{3+}, Ho^{3+}, Eu^{3+}, Nd^{3+}) powder was synthesized by conventional solid state reactions with stoichiometric ratios of $CaCO_3$ (99.99 % purity), γ-Al_2O_3 (99.99 % purity), Y_2O_3 (99.99 % purity), Ho_2O_3 (99.9 % purity), Eu_2O_3 (99.9 % purity) and Nd_2O_3 (99.9% purity) powders at 1200 °C for 12 h in O_2 atmosphere. The resulting powder was confirmed to be single phase C12A7 based on powder X-ray diffraction (XRD) analysis. To make the feed rod, the fine powder was transferred to a rubber tube and pressed under 300 MPa hydrostatic pressure and subsequently sintered at 1300 °C for 12 h in O_2 atmosphere to obtain a high density feed rod, which was also used as a seed.

An optical-focusing floating zone furnace (FZ-T-10000-H-III-VPS-YT, Crystal Systems Inc., Japan) equipped with four 1000 W halogen lamps was used to carry out crystal growth. Bubble-free crystals were grown at a growth rate of 1 mm·h^{-1} in an O_2 atmosphere of 0.1 MPa pressure. At the end of growth, the molten zone was slowly cooled and then detached from the feed. The dopant concentration in the cone-shaped final part of the grown crystals was measured by EPMA to determine the solubility limit of Ln^{3+} in the C12A7 phase. To determine distribution coefficients, C12A7:Ln crystals were grown at a rate of 1 mm·h^{-1} using feeds having dopant concentrations lower than the solubility limit in order to prevent precipitation of the second phase. We measured the Ln concentration along the growth direction at the central and peripheral regions in the grown crystals, and from these data, the effective distribution coefficients of Ln^{3+} into C12A7 were determined.

4. Determination of solubility limit of Ln^{3+} in C12A7

4.1 Solubility from zone melt growth

To determine the solubility limit, Ln^{3+}-doped C12A7 crystals were grown at a rate of 1 mm·h^{-1} using 1 and 2 at% Ln^{3+}-doped C12A7 feeds. The as-grown of 1 at% Ho-doped C12A7 and SEM image of the of the final part of grown crystal C12A7:Ho were shown in Fig.2. A eutectic structure with Ho-rich phase and $CaAl_2O_4$ (CA) phase besides the C12A7 phase was observed in the final part of the grown crystal. Thus the Ln concentration in only C12A7 phase in the final growth region of the crystals was determined along the crystal growth direction by EPMA as shown in Fig.3. In Figs.3(a) and 3(b), the Y^{3+} concentration in C12A7:Y increases slightly along the growth direction and becomes nearly constant in the final region of about 2 mm from the crystal edge, and the maximum concentration is 0.29 at% and 0.31 at% when using 1 and 2 at% Y-doped feeds, respectively. For Ho-doping, the maximum Ho concentration in C12A7:Ho is nearly identical for both 1 and 2 at% Ho-doped feeds, even though the Ho concentration along the growth direction in C12A7:Ho fluctuates slightly [Figs.3(c) and 3(d)]. For 1 and 2 at% Eu- and 1 at% Nd-doping, the obtained dopant concentration increases from the measurement point (zero along the growth

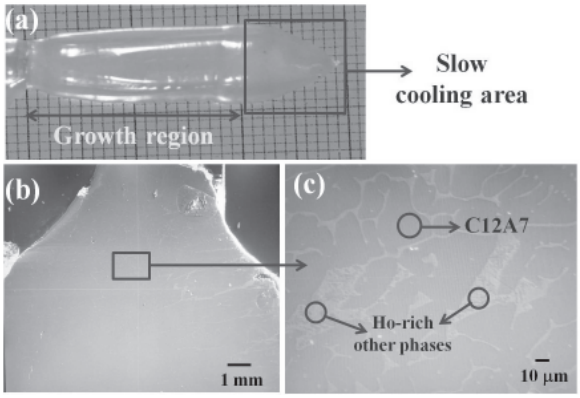

Fig.2 1 at% Ho-doped C12A7:Ho grown crystal (a), the SEM image of the final part of grown crystal C12A7:Ho (b) and expanded SEM image of the final part (c).

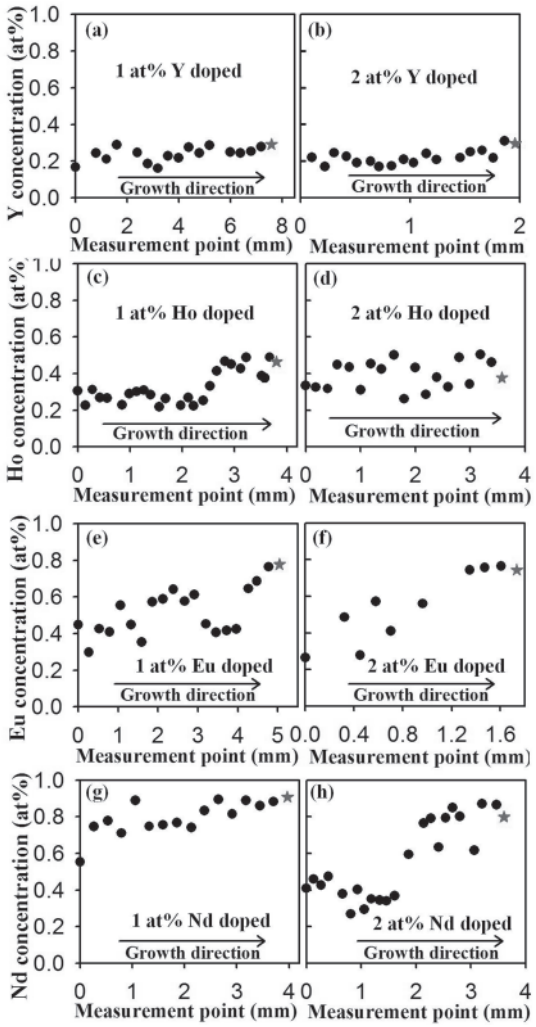

Fig.3 Dopant concentration along the growth direction at the final growth region in the crystals grown by using feeds containing 1 or 2 at% Y^{3+} (a,b), Ho^{3+} (c,d), Eu^{3+} (e,f) and Nd^{3+} (g,h) doped C12A7. Zero on the abscissa and asterisk (*) mark data indicate the starting point along growth direction and edge point of measurement.

direction) to the growth direction, reaching a maximum along the top region.

In the case of 2 at% Nd-doping, the Nd concentration in C12A7:Nd sharply increased to almost the same maximum dopant concentration in the final part as in the case of 1 at% Nd-doping. The maximum dopant concentration of Ln in C12A7 in the final part of the grown crystals was nearly identical, and saturated even though the dopant concentration in the feed was increased from 1 at% to 2 at% as shown in Table 1. Thus, we are getting almost same maximum dopant concentration for 1 at% and 2 at% Ln-doped feeds and hence, we have estimated the solubility limit of Ln^{3+} in the C12A7 phase by taking the average of the measured maximum dopant concentration data. The coordination number (CN) of both Ln^{3+} and Ca^{2+} is six, but the ionic radii of Ln^{3+} ions are much larger than that of Al^{3+} (0.039 nm, CN = 4) and nearly equivalent to the ionic radius of Ca^{2+} (0.099 nm) (Table 1). Therefore, it is reasonable to suggest that all Ln^{3+} ions preferentially substitute for Ca^{2+} in C12A7.

Table 1 The maximum dopant concentration and the estimated solubility limit of Ln^{3+} into C12A7:Ln crystal for 1 and 2 at% Ln^{3+} doped C12A7 feed and ionic radius of Ln^{3+} ions quoted from the ref [22].

Ion	Ionic Radii (nm)	Maximum dopant in C12A7:Ln crystal (at%)		Estimated solubility limit (at %)
		1 at% doped feed	2 at% doped feed	
Y^{3+}	0.0900	0.29	0.31	0.30(1)
Ho^{3+}	0.0901	0.47	0.50	0.48(2)
Eu^{3+}	0.0947	0.78	0.77	0.78(1)
Nd^{3+}	0.0983	0.91	0.90	0.91(1)

The obtained maximum dopant concentration and estimated solubility limit of Ln^{3+} ions in the Ca^{2+} site of C12A7 are shown in Fig.4 and Table 1. In Fig.4, the maximum dopant concentrations for 1 at% Ln^{3+} doping (open circles) coincide with the same values for 2 at% Ln^{3+} doping (pink triangles), which indicates that the solubility limit of Ln^{3+} should be within the range of these maximum dopant concentrations, and will not change at further high doping levels. The maximum dopant concentration of Ln^{3+} increases in a linear fashion with respects to ionic radius even though the maximum dopant concentration of Ho^{3+} is higher than that of Y^{3+} in spite of same ionic radius. The exact reason is not known to us. The solubility limit might be related to the strength of the covalent bond for Ln^{3+}, since the covalent radius of Ho^{3+} (0.192 nm) is greater than that of Y^{3+} (0.190 nm)[23].

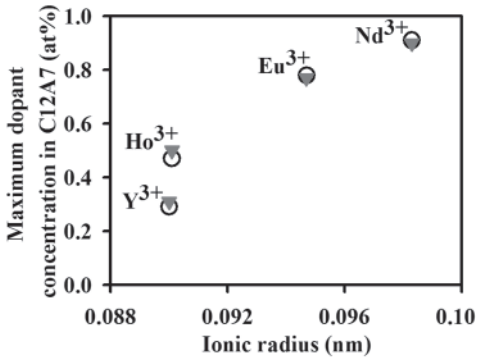

Fig.4 Maximum dopant concentrations in C12A7:Ln crystals as a function of dopant ionic radius. Open circles and closed triangles represent maximum dopant concentrations for 1 and 2 at% Ln doping, respectively.

4.2 Conventional determination of solubility limit

To confirm the solubility limits determined by FZ growth, the solubility limit of Y^{3+} in C12A7 was also determined using a conventional solid state reaction method. C12A7:Y polycrystalline powder was prepared with various nominal Y concentrations by a solid state reaction at 1200 °C for 24 h in oxygen atmosphere. The powder XRD pattern of the synthesized powder was obtained at a scan speed of 0.5 °·min^{-1} with a step angle of 0.002 ° using a receiving slide 0.15 nm wide and Cu *K*α X-ray radiation. Figures 5(a) and 5(b) show the XRD patterns and the lattice parameters for C12A7:Y samples doped with 0.0−2.0 at% Y. Here, the diffraction peaks shifted to higher angles as the Y concentration in the C12A7:Y samples increased, indicating decreased lattice parameters.

The positions of the diffraction peaks did not change significantly from 0.3 to 2 at% Y-doping, indicative of a constant lattice parameter [Fig.5(b)]. The solubility limit of Y in the synthesized C12A7:Y polycrystalline sample was estimated to be approximately 0.3 at%, in agreement with the crystal obtained by FZ growth. Determining the solubility limit in synthesized C12A7:Ln polycrystalline powders by conventional solid state reaction methods is fairly complex and time consuming. However, determining these parameters from FZ growth data obtained from C12A7:Ln crystals is both reliable and straightforward.

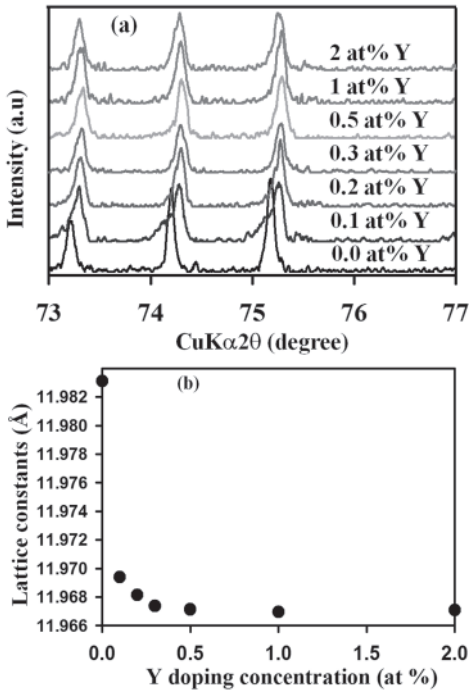

Fig.5 XRD patterns (a) and calculated unit cell lattice parameters in C12A7:Y prepared samples with nominal concentration of 0.0, 0.1, 0.2, 0.3, 0.5, 1 and 2 at% Y respectively (b).

5. Determination of distribution coefficient of Ln^{3+} in C12A7

5.1 Dependence of the radial position on Ln distribution in the C12A7:Ln grown crystals

The dopant distribution along the growth direction at the initial growth region in the crystals grown by FZ method is required to determine the distribution coefficient of Ln in C12A7. However, the homogeneity of the dopant concentration in the radial direction is strongly dependent on the growth interface. We have measured the Nd concentration along the growth direction in the central and peripheral areas of the crystal grown at a rate of 1 mm·h^{-1} using a feed containing 0.50 at% Nd-doped C12A7 as shown in Fig.6(a). The

Nd concentration in the central area of the grown crystals along the growth direction is higher than that of the peripheral area. To explain this inhomogeneous dopant concentration, we took an EPMA map of the growth interface shape by quenching the molten zone during FZ growth of 0.50 at% Nd-doped C12A7 crystals. The growth interface shape of Nd-doped C12A7 was concave as shown in Fig.6(b). The concave interface shape enhances the dopant concentration along the core of the growing crystals. The low thermal conductivity in the melt may promote the formation of this concave interface shape, although the exact material parameters are still unknown [24].

During FZ growth using an infrared radiation convergence-type furnace, the growth interface of the oxide materials absorbs very little near-infrared radiation, which tends to form concave shapes in the melt [25]. This concave interface shape may also be influenced by the Marangoni convection, driven by the gradient of surface tension at the free liquid surface [26]. A surface tension gradient occurs because of the temperature or dopant concentration gradient in the melt. The inhomogeneity of the Nd concentration along the growth direction may be one of the reasons for this concave interface shape. Thus, there is room for further studies to minimize the concave solid liquid interface shape to obtain homogenous dopant concentrations in single crystals. In the schematic diagram of initial crystallization [Fig.6(c)], the molten zone is highly concave. Due to this concave interface shape, initial crystallization starts from the peripheral area, while at the same time along the radial direction the center area is still in a melt state. This means that the center area crystallizes later compared to the peripheral area along the same radial direction. As initial crystallization at the peripheral area occurs earlier than in the central area along the same radial direction, the dopant concentration in the central area of the melt will be different from the concentration in the initial melt. As a result, the distribution coefficient at the initial growth position in the peripheral area will be more reliable than in the central area. Hence, we have determined the effective distribution coefficient in the peripheral area of the grown crystals.

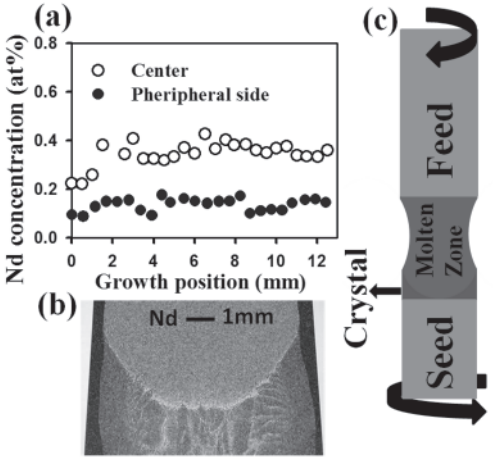

Fig.6 Nd concentration along the growth direction at the central and peripheral areas of a crystal grown using a 0.5 at% Nd-doped feed (a) Nd concentration map at growth interface (b), and the schematic diagram of initial crystallization (c).

5.2 Distribution coefficient

The distribution of dopant concentration C from the initial crystallization point along the growth direction in the periphery of a C12A7:Ln crystal grown using a Ln-doped feed of concentration C_0 (0.27, 0.34, 0.50 and 0.50 at% Y, Ho, Eu and Nd) was measured by EPMA. The relative salute concentration, C/C_0 with respect to travelled molten zone length, x/l is shown in Fig.7(a).

The equation (1) as described above can be simplified as:

$$ln\left(1-\frac{C(x)}{C_0}\right) = -k\frac{x}{l} + ln(1-k) \qquad (2)$$

The distribution coefficient k is estimated from the negative slope and intersects of equation (2). Figure 7(b) shows $ln(1-C(x)/C_0)$ *vs.* x/l plots for Nd, Ho, Y and Eu in C12A7:Ln crystals grown at a rate of 1 mm·h^{-1} while maintaining a molten zone length l of approximately 9 mm. Thus, by using equation (2) the effective distribution coefficients k of Nd, Ho, Y and Eu were estimated to be 0.142 ± 0.015, 0.108 ± 0.011, 0.105 ± 0.012 and 0.075 ± 0.007, respectively.

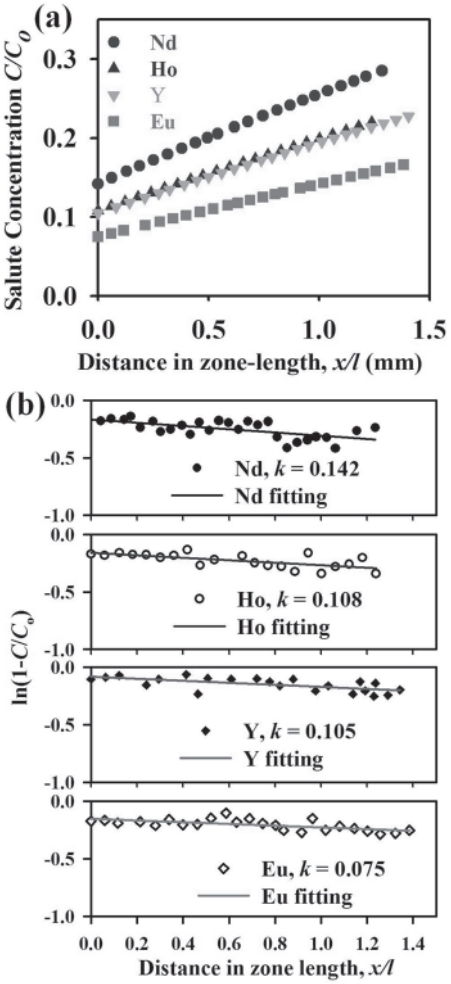

Fig.7 The relative Ln concentration, C/C_0 with C_0 = 0.27, 0.34, 0.50 and 0.50 at% for Y, Ho, Eu and Nd respectively (a) and effective distribution coefficient of Ln along travelled molten zone length x/l (b).

6. Summary

Rare earth ion Ln^{3+} (Ln = Y, Ho, Eu or Nd)-doped bubble-free C12A7:Ln crystals have been grown at a growth rate of 1 mm·h^{-1} by a FZ method in the atmosphere of 0.1 MPa O_2. The maximum dopant concentration of Ln in C12A7 in the final growth region of the crystals using feeds of 1 and 2 at% Ln-doped C12A7 was investigated by EPMA to estimate the solubility limit. The solubility limits of Y, Ho, Eu and Nd ions in the C12A7:Ln crystals were estimated to be 0.30(1), 0.48(2), 0.78(1) and 0.91(1) at%, respectively. The solubility limit of Y determined using FZ melt growth was in good agreement with the same limit determined using a more conventional solid state reaction method. The distribution of

dopant concentration along the growth direction at the initial growth region in the periphery of the grown C12A7:Ln crystal was studied using 0.27, 0.34, 0.50 and 0.50 at% Y, Ho, Eu, and Nd-doped C12A7 feeds. The effective distribution coefficients of Y, Ho, Eu, and Nd into C12A7 crystal grown at a rate of 1 $mm \cdot h^{-1}$ was determined to be 0.105(12), 0.108(11), 0.075(7) and 0.142(15), respectively. Based on these data, we suggest that determining solubility limits and distribution coefficients using FZ growth methods is quite easy and reliable.

Acknowledgment

This work was supported in part by a Grant-in-Aid for Scientific Research (C) JP25420708 from the Japan Society for the Promotion of Science (JSPS). M. M. Ali was supported by a Japanese Government Scholarship from The Ministry of Education, Culture, Sports, Science and Technology (MEXT).

References

1) H. F. W. Taylor, *The Chemistry of Cements*, Academic Press, London, **1964**.
2) R. J. Mangabhai, F. P. Glasser (Eds.), *Calcium Aluminate Cements*, The University Press, Cambridge, U.K., **2001**.
3) R. W. Nurse, J. H. Welch, A. J. Majumdar, *Trans. Brit. Ceram. Soc.*, **1965**, *64*, 323.
4) J. A. Imlach, L. S. D. Glasser, F. P. Glasser, *Cem. Concr. Res.*, **1971**, *1*, 57.
5) J. Jeevaratnam, F. P. Glasser, L. S. D. Glasser, *J. Am. Ceram. Soc.*, **1964**, *47*, 105.
6) M. Miyakawa, H. Kamioka, M. Hirano, T. Kamiya, P. V. Sushko, A. L. Shluger, N. Matsunami, H. Hosono, *Phys. Rev. B*, **2006**, *73*, 205108.
7) S. Matsuishi, Y. Toda, M. Miyakawa, K. Hayashi, T. Kamiya, M. Hirano, I. Tanaka, H. Hosono, *Science*, **2003**, *301*, 626.
8) S. W. Kim, S. Matsuishi, T. Nomura, Y. Kubota, M. Takata, K. Hayashi, T. Kamiya, M. Hirano, H. Hosono, *Nano Lett.*, **2007**, *7*, 1138.
9) M. Miyakawa, S. W. Kim, H. Hirano, Y. Kohama, H. Kawaji, T. Atake, H. Ikegami, K. Kono, H. Hosono, *J. Am. Chem. Soc.*, **2007**, *129*, 7270.
10) S. W. Kim, M. Miyakawa, M. Hirano, Y. Kohama, H. Kawaji, T. Atake, H. Ikegami, K. Kono, H. Hosono, *Mater. Trans.*, **2008**, *49*, 1748.
11) M. Lacerda, J. T. S. Irvine, F. P. Glasser, A. R. West, *Nature*, **1988**, *332*, 525.
12) J. T. S. Irvine, M. Lacerda, A. R. West, *Mater. Res. Bull.*, **1988**, *23*, 1033.
13) K. Hayashi, S. Matsuishi, T. Kamiya, M. Hirano, H. Hosono, *Nature*, **2002**, *419*, 462.
14) K.-B. Kim, M. Kikuchi, M. Miyakawa, H. Yanagi, T. Kamiya, M. Hirano, H. Hosono, *J. Phys. Chem. C*, **2007**, *111*, 8403.
15) Y. X. Liu, L. Ma, D. T. Yan, H. C. Zhu, X. L. Liu, H. Y. Bian, H. Zhang, X. J. Wang, *J. Lumines.*, **2014**, *152*, 28.
16) X. Liu, Y. Liu, D. Yan, H. Zhu, C. Liu, C. Xu, Y. Liu, X. Wang, *J. Mater. Chem.*, **2012**, *22*, 16839.
17) R. Wang, L. Liu, J. Sun, Y. Qian, Y. Zhang, Y. Xu, *Opt. Commun.*, **2012**, *285*, 957.
18) Y. Qu, R. Wang, L. Liu, J. Sun, L. Xing, Y. Tao, X. Wu, *Cryst. Res. Technol.*, **2013**, *48*, 1031.
19) H. Zhu, Y. Liu, D. Yan, H. Bian, S. Li, C. Liu, C. Xu, X. Wang, *Opt. Mater.*, **2014**, *36*, 1771.
20) W. Pfann, *Zone Melting, 2nd ed*, Wiley, New York, **1966**.
21) I. Tanaka, *J. Tech. Assoc. Refract. Jpn*, **2013**, *33*, 18.
22) R. D. Shannon, C. T. Prewitt., *Acta Crystallogr. B*, **1969**, *25*, 925.
23) B. Cordero, V. Gómez, A. E. Platero-Prats, M. Revés, J. Echeverría, E. Cremades, F. Barragán, S. Alvarez, *Dalton Trans.*, **2008**, 2832.
24) K. Kitamura, S. Kimura , S. Hosoya, *J. Cryst. Growth*, **1980**, *48*, 469.
25) K. Kitamura , S. Kimura , K. Watanabe, *J. Cryst. Growth*, **1982**, *57*, 475.
26) Thierry Duffar (Ed.), *Crystal Growth Processes Based on Capillarity*, Wiley, **2010**.